Thermal characterization of single-wall carbon nanotube bundles using the self-heating 3ω technique

Jinbo Hou, Xinwei Wang,[a] Pallavi Vellelacheruvu, and Jiaqi Guo
Department of Mechanical Engineering, N104 Walter Scott Engineering Center, University of Nebraska-Lincoln, Lincoln, Nebraska, 68588-0656

Chang Liu and Hui-Ming Cheng
Shenyang National Laboratory for Materials Science, Institute of Metal Research, Chinese Academy of Sciences, Shenyang 110016, People's Republic of China

(Received 11 July 2006; accepted 17 October 2006; published online 28 December 2006)

In this work, we have developed a complete solution for the thermal transport in single-wire based 3ω experiment and have studied the effect of radiation on the experiment. Microscale Pt wires are used as the reference sample to measure its specific heat and thermal conductivity. Sound agreement between the measurement data and reference values is obtained. A series of experiments is conducted to characterize the thermal transport property of single-wall carbon nanotube (SWCNT) bundles. The average thermal diffusivity measured for three different SWCNT bundles is around 1.74×10^{-5} m^2/s, much less than the thermal diffusivity of bulk graphite in the layer direction. Physical reasons for this low thermal diffusivity are discussed based on our structure study of the SWCNT bundles. © *2006 American Institute of Physics*. [DOI: 10.1063/1.2402973]

I. INTRODUCTION

The development of microelectromechanical systems (MEMSs) and nanoelectromechanical systems (NEMSs) predicts outstanding significance in the technological world and every part of human life. For these extremely small systems, their components play a significant role in their performance and function. To better control and optimize the system functionality, knowledge about the physical properties of the components in the system becomes extremely important.

A wide variety of unique physical properties[1–5] of carbon nanotubes (CNTs) makes them applicable as the basic components of MEMS and NEMS. In general nanostructures, due to their low dimensions, they exhibit much reduced thermal conductivity because of increased boundary scattering and modified phonon dispersion.[6,7] But CNTs exhibit high thermal conductivity because of their crystalline structure, where the boundary scattering is almost absent, and due to their large phonon mean path.[8]

In the past, microfabricated devices[9] and many conventional techniques[10–14] have been developed to study the thermal conductivity of CNTs and thin films[15–17] at the nanometer level. Difficulties may arise due to thermal radiation, heat loss in the measuring probes, and accuracy in measuring the power supply. One of the methods, the 3ω technique, overcomes the above difficulties using the specimen as both heater and thermometer which is closely related to hot wire[18,19] and hot strip methods.[20] Though initially the 3ω method was developed to measure the properties of amorphous bulk materials with low and high thermal conductivities, later it was applied for thin films and nanowires/nanotubes. This method uses narrow band detection technique, resulting in a better signal to noise ratio. In this technique, the sample is considered as a thermometer if it is electrically conductive and if its resistance changes with temperature. An ac current of ω frequency is supplied to the sample, which creates a temperature fluctuation at 2ω, finally leading to a 3ω voltage fluctuation across the specimen. This 3ω fluctuation in the specimen embodies the information about the thermophysical properties of the material. Experiments were performed further to study the details of the method.[12,21] Choi *et al.*[22] discoursed about the microelectromechanical system technology to connect single multiwalled CNTs between two electrodes and then used the 3ω method to find the thermal conductivity.

In the 3ω technique to measure the thermal conductivity of individual one-dimensional nanostructures, due to the large aspect ratio of the sample, the radiation heat loss from the sample surface could have a strong effect on the experimental results. In addition, due to the small size of the sample, the heat transfer in the connected electrodes can affect the result to a great extent. All these effects are well explored in this work for freestanding wire-based 3ω technique.

In Sec. II, we will present the theoretical solution for the thermal transport in a single wire connected between two electrodes. In this solution, the three-dimensional (3D) heat transfer in the electrode base is taken into account. In Sec. III, we will discuss how the radiation heat transfer affects the experimental results. Section IV constitutes three sections: a brief explanation about the experimental setup, system calibration using platinum (Pt) wires, and structure and thermal characterizations of single-wall carbon nanotube (SWCNT) bundles.

II. PHYSICAL MODEL DEVELOPMENT

In the self-heating 3ω experiment, a thin conductive wire is connected between two bases. In our experiment, the

[a]Author to whom correspondence should be addressed; FAX: (402) 472-1465; electronic mail: xwang3@unl.edu

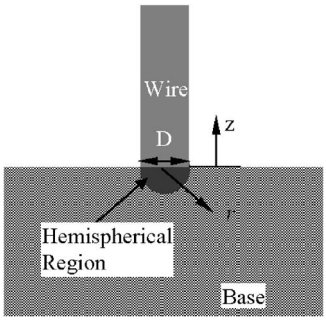

FIG. 1. Schematic of the interface treatment between the wire and the base for heat transfer analysis.

modulation frequency of the current passing through the wire will be carefully selected to make the thermal diffusion length $\mu=\sqrt{2\alpha/f}$ (α: thermal diffusivity of the wire; f: modulation frequency) much larger than the wire diameter D. As a result, it is physically reasonable to assume that the wire has a uniform temperature distribution in its cross section. Only the heat transfer along the axial direction of the wire needs to be considered. The heat transfer problem of interest will be divided into two parts: one part is the heat transfer along the wire (z direction, as shown in Fig. 1), and the other part is the heat transfer in the bases. Solutions to these two parts will be combined using the boundary conditions at $z=0$. In the experiment, the electrical heating power has the form of $I_0^2\cos^2(\omega t)R=1/2I_0^2R[1+\cos(2\omega t)]$.

For thermal transport in the wire, the complex governing equation follows

$$\frac{\partial(\rho c_p T)}{\partial t}=k\frac{\partial^2 T}{\partial z^2}+Q_0e^{2i\omega t}+Q_0, \tag{1}$$

where $Q_0=I_0^2R/2LS$. L, S, and R are the length, cross-sectional area, and resistance of the wire, respectively. I_0 is the amplitude of the modulated electrical current. ρ, c_p, and k are the density, specific heat, and thermal conductivity of the wire, respectively. The solution T to Eq. (1) consists of three parts: the transient component T_t, which reflects the temperature change at the early stage of electrical heating, the final temperature elevation $\bar{T}_s$ due to the electrical heating, and the steady transient component $\tilde{T}_s$, which varies with time periodically. In the 3ω measurement, the lock-in amplifier only picks up the signal periodically varying with time. Therefore, only $\tilde{T}_s$ needs to be evaluated here. $\tilde{T}_s$ results from the periodical source term $Q_0\exp(2i\omega t)$ in Eq. (1). When only this source term is considered, Eq. (1) has a particular solution in the form of $\tilde{T}_s=\theta e^{2i\omega t}$. Substituting this particular solution in Eq. (1), we readily find that θ has the form of

$$\theta=\frac{Q_0}{\rho c_p 2i\omega}+C_1e^{\sqrt{A}z}+C_2e^{-\sqrt{A}z}, \tag{2}$$

where $A=\rho c_p 2i\omega/k$. To simplify the expression in the derivation, we take $B=Q_0/(\rho c_p 2i\omega)$. Since the heat transfer in the wire is symmetric with respect to the location of $z=L/2$, only the heat transfer in the range of $z=0\sim L/2$ will be evaluated. At $z=0$, the wire temperature is assumed to be $T_0e^{2i\omega t}$. T_0 will be solved later based on the interface boundary condition at $z=0$. Consequently, we have boundary conditions of $\partial\theta/\partial z=0$ at $z=L/2$ and $\theta=T_0$ at $z=0$. Substituting the boundary conditions into Eq. (2), C_1 and C_2 are solved as $C_1=(T_0-B)/(1+e^{\sqrt{A}L})$ and $C_2=(T_0-B)/(1+e^{-\sqrt{A}L})$.

The heat transfer rate q at the interface between the wire and the base ($z=0$) (as shown in Fig. 1) is evaluated as

$$q=-k\left[\pi(D/2)^2\frac{\partial\theta}{\partial z}\right]_{z=0}$$
$$=-k\pi(D/2)^2\sqrt{A}(T_0-B)\frac{1-e^{\sqrt{A}L}}{1+e^{\sqrt{A}L}}. \tag{3}$$

As stated before, the modulation frequency will be carefully selected to make $\mu=\sqrt{2\alpha/f}\gg D$ for the wire. In the 3ω experiment, the base material is a sound thermal conductor and has high thermal conductivity. Therefore, this condition ($\mu=\sqrt{2\alpha/f}\gg D$) also applies for the base. As a result, we can assume that the small hemispherical region, as shown in Fig. 1, has a uniform temperature of $T_1e^{2i\omega t}$. The simplification makes it possible to obtain an analytical solution for the whole system. In our experiment, silver paste is used to connect the to-be-measured wire with the base, and the end of the wire is embedded in the paste. The wire-based contact shown in Fig. 1 clearly represents this structure. For the base, the heat transfer will become one dimensional in the spherical coordinate, as shown in Fig. 1. The governing equation for this heat transfer is

$$\frac{\partial\rho_b c_{p,b}T_b}{\partial t}=k_b\frac{1}{r^2}\frac{\partial}{\partial r}\left(r^2\frac{\partial T_b}{\partial r}\right), \tag{4}$$

where ρ_b, $c_{p,b}$, and k_b are the density, specific heat, and thermal conductivity of the base, respectively. Again, we only need to solve the steady transient component of the temperature $\tilde{T}_{s,b}$, which varies with time periodically. Letting $\tilde{T}_{s,b}=\theta_b e^{2i\omega t}$, we can obtain

$$\theta_b=\frac{1}{r}(C_3e^{\sqrt{A_1}r}+C_4e^{-\sqrt{A_1}r}), \tag{5}$$

where $A_1=\rho_b c_{p,b}2i\omega/k_b$. When $r\to\infty$, θ_b will become negligible. Therefore, we have $C_3=0$. If we assume the at $r=r_0$ and $\theta_b=T_1$, we have $C_4=T_1e^{\sqrt{A_1}r_0}r_0$. The heat transfer rate at $r=r_0$ is expressed as

$$q_b=2\pi r_0^2\left(-k_b\frac{\partial\theta_b}{\partial r}\right)_{r=r_0}=2\pi r_0^2k_bT_1\left(\frac{1}{r_0}+\sqrt{A_1}\right). \tag{6}$$

Up to this point, for the temperature distributions in the wire [Eq. (2)] and the base [Eq. (5)], only two parameters are to be determined: T_0 and T_1. In order to determine them, two interface boundary conditions are used $q_b=-q$ and $\pi r_0^2(T_0-T_1)/R''_{tc}=q_b$. Here R''_{tc} is the thermal contact resistance between the wire and the base. Using these two interface conditions, T_0 and T_1 are determined as

$$T_0=\frac{U_1B(1+U_2)}{U_1(1+U_2)-1}, \tag{7}$$

$$T_1 = \frac{U_1 B}{U_1(1+U_2)-1}, \tag{8}$$

where $U_1 = k\sqrt{A}(1-e^{\sqrt{A}L})/\{(1+e^{\sqrt{A}L})[2k_b(r_0^{-1}+\sqrt{A_1})]\}$ and $U_2 = R''_{tc}2k_b(r_0^{-1}+\sqrt{A_1})$. We are interested in the average temperature ($\bar{\theta}$) of the wire. By integrating Eq. (2) along the z direction, we can easily find $\bar{\theta}$ as

$$\bar{\theta} = \frac{1}{L/2}\int_0^{L/2} \theta dz = B + \frac{2}{L}\left[\frac{1}{\sqrt{A}}(C_1 e^{\sqrt{A}L/2} - C_2 e^{-\sqrt{A}L/2}) + \frac{1}{\sqrt{A}}(C_2 - C_1)\right]. \tag{9}$$

The average temperature $\bar{\tilde{T}}_s$ (in complex form) along the wire is calculated as $\bar{\tilde{T}}_s = \bar{\theta}e^{2i\omega t} = \bar{\theta}_m e^{i(2\omega t+\phi)}$, where $\bar{\theta}_m$ and ϕ are the amplitude and phase shift of $\bar{\theta}$, respectively.

It has to be pointed out that only the real part of $\tilde{T}_s$ is the solution to the heat transfer in the wire. Namely, we can only use the real part of $\bar{\tilde{T}}_s$ and $\bar{\theta}_m \cos(2\omega t+\phi)$ to get the 3ω voltage across the wire. Finally, as a component of the product of $\bar{\theta}_m \cos(2\omega t+\phi)$ and $I_0 \cos(\omega t)$, the 3ω voltage across the wire is

$$V_{3\omega} = \frac{1}{2}\bar{\theta}_m \frac{dR}{dT} I_0 \cos(3\omega t + \phi). \tag{10}$$

III. EFFECT OF RADIATION HEAT TRANSFER

In Eq. (1), the radiation heat loss from the surface of the wire is not considered. For thin wires, because of their large aspect ratio, the radiation heat loss could have a strong effect on the measurement result. Considering thermal radiation at the wire surface, the governing equation for the heat transfer in the wire is modified as

$$\frac{\partial(\rho c_p T)}{\partial t} = k\frac{\partial^2 T}{\partial z^2} + Q_0 e^{2i\omega t} + Q_0 - \frac{\pi D L \varepsilon \sigma (T^4 - T_{sur}^4)}{\pi D^2 L/4}, \tag{11}$$

where ε and σ are the surface emissivity and the Stefan-Boltzmann constant, respectively. T_{sur} is the surrounding ambient temperature. For structures with feature/characteristic size of a few hundreds of nanometers or smaller, the emission from the surface will be strongly affected by the structure dimension, and the emission will favor a certain spectrum range. Therefore, the concept of emissivity and blackbody emission used in Eq. (11) will be less accurate. The treatment of the surface radiation heat transfer in Eq. (11) is to provide the first order estimation of the radiation effect on the experiment. Our following analysis and calculation represent an extreme situation and will place the estimation on the safe side to make sure that in this experiment, the radiation heat loss from the wire will be negligible. In our recent transient experiment for nanoscale polymer wires (~400 nm diameter), it is found that the radiation effect from the wire surface significantly distorted the experiment and led to unreasonably high thermal conductivity. Therefore, the purpose of the radiation effect analysis in the work is to point out that for the samples measured in the paper, the radiation effect is negligible. For wires with diameters of a few hundreds of nanometers or even thinner, great caution should be exercised to reduce the radiation heat transfer effect.

TABLE I. Properties of Pt wire and copper (300 K)

	Pt wire	copper
Length (mm)	10.0	
Density (kg/m^3)	2.145×10^4	8.933×10^3
Specific heat (J/kg K)	133	385
Electrical resistivity (Ω m)[a]	0.1086×10^{-6}	
α (Ω/K)[a]	0.003 927	
Thermal conductivity (W/m K)	71.6	401

[a]These properties from Ref. 23. At 300 K, the electrical resistivity of Pt is $0.106\times10^{-6}/[1+(293.15-273.15)\times0.003\,927]\times[1+(300-273.15)\times0.003\,927]=0.1086\times10^{-6}$ Ω m.

As stated before, $T = T_t + \bar{T}_s + \tilde{T}_s$. In steady state $T_t = 0$, so $T = \bar{T}_s + \tilde{T}_s$. Because $\tilde{T}_s << \bar{T}_s$, to the first order approximation, we have $T^4 = \bar{T}_s^4 + 4\bar{T}_s^3\tilde{T}_s$. Substituting it into Eq. (11), we can obtain two separate equations for the dc and ac temperature components. We are only interested in the component periodically varying with time, $\tilde{T}_s$. Letting $\tilde{T}_s = \theta e^{2i\omega t}$, we can have

$$\theta\left(\rho c_p 2i\omega + \frac{16\varepsilon\sigma\bar{T}_s^3}{D}\right) = k\frac{\partial^2\theta}{\partial^2 z} + Q_0. \tag{12}$$

It is readily found that the solution to Eq. (12) has the same form as Eq. (2). Therefore, the solution developed for Eq. (1) can be used for Eq. (12) as well by replacing $\rho c_p 2i\omega$ with $\rho c_p 2i\omega + 16\varepsilon\sigma\bar{T}_s^3/D$ in Eq. (2).

As analyzed before, when the wire diameter becomes small, the radiation could influence the 3ω signal to a great extent. In order to find out how the radiation effect varies with diameter, several cases are studied with different wire diameters. The wire material and base material are Pt and copper, respectively. Their properties are given in Table I.[23,24] The thermal contact resistance takes 1.0×10^{-9} m^2 K/W. In real experiments, the temperature elevation of the wire is controlled to be moderate. Therefore, in this calculation, the steady temperature $\bar{T}_s$ in Eq. (12) is chosen to be room temperature, 300 K. The voltage applied to the Pt wire is assumed to be 28 μV based on our experiment. To explore the extreme situation of the radiation influence, the emissivity of the Pt wire is set to 1.

Before studying the effect of radiation heat loss, the effect of wire diameter on the phase shift and amplitude of the 3ω signal is studied first for typical experimental frequencies. It was found that without considering the radiation heat loss, the phase shift and amplitude of the 3ω signal is almost independent of the wire thickness. For the effect of radiation on the phase shift and amplitude of the 3ω signal, Pt wires of different diameters are studied. These calculation results are summarized in Fig. 2. In the above calculations, it is found

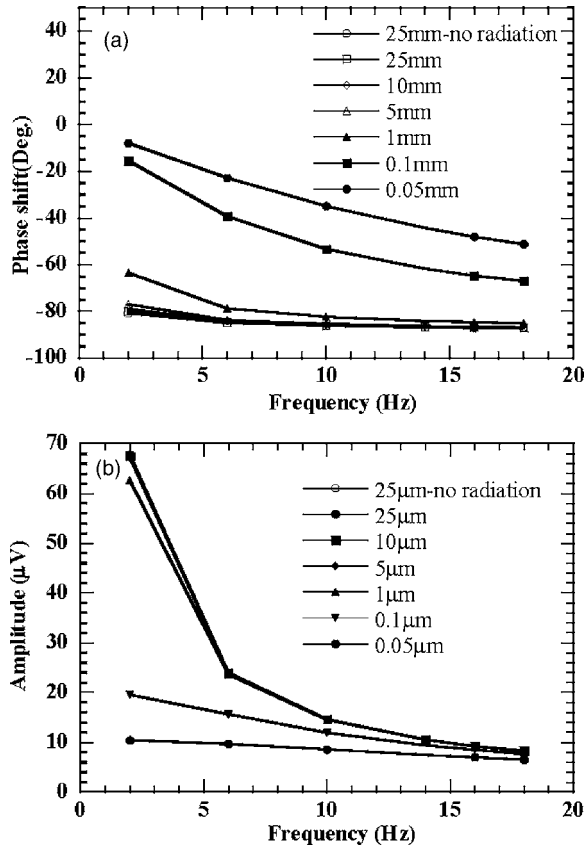

FIG. 2. Phase shift (a) and amplitude (b) with consideration of the radiation heat loss for Pt wires of different diameters at the same length (1 cm). For comparison, the phase shift without considering radiation (25.4 μm, no radiation) is also shown in the figure.

that the diameter of the wire has little effect on the phase shift and amplitude of the 3ω signal. Therefore, the differences in the phase shift and amplitude for wires of different diameters shown in Fig. 2 are solely attributed to the surface radiation heat loss. Figure 2 shows that if radiation is considered, the amplitude and phase shift (its absolute value) of the 3ω signal both decrease with the decreasing wire diameter, especially when the wire diameter is less than 1 μm. Therefore, for wires (1 cm long) less than 1 μm thick, the radiation heat loss has a strong effect on the 3ω signal and needs to be taken into account, especially for low frequencies.

The ratio of the radiation heat loss to the heat conduction along the wire is approximately proportional to $A_{\text{sur}}/A_{\text{cross}} = 4L/D$, where A_{sur} and A_{cross} are the surface and cross-sectional areas of the wire, respectively. It is obvious that when the diameter D of the wire is smaller, this ratio becomes larger, meaning radiation heat loss from the surface becomes more important. Therefore, for thinner wires, the amplitude of the 3ω signal becomes smaller because of the radiation heat loss. This trend can also be explained by the term $\rho c_p 2i\omega + 16\varepsilon\sigma\bar{T}_s^3/D$ used in Eq. (12). Comparing the solution of Eq. (12) and Eq. (2), the effect of the radiation can be treated by the change of ρc_p to $\rho c_p + 8\varepsilon\sigma\bar{T}_s^3 i/(\omega D)$, namely, $(\rho c_p)_{\text{effective}}$. When the wire diameter is smaller, the absolute value of the effective ρc_p becomes larger, leading to a smaller amplitude of the 3ω signal. The radiation heat loss

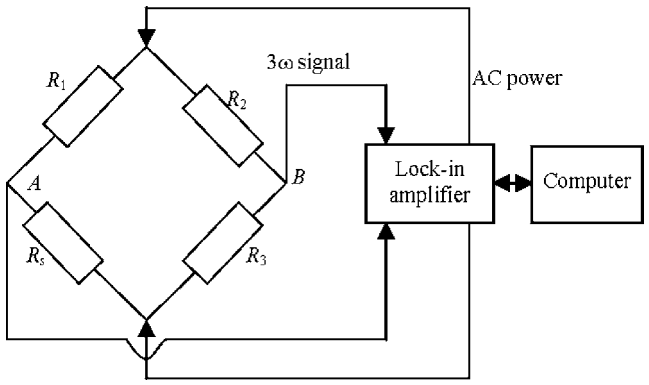

FIG. 3. Schematic of the 3ω experimental setup with the Wheatstone bridge and using a lock-in amplifier as the ac power source.

from the wire surface reduces the temperature increasing rate during current heating, making the peak location of temperature closer to the peak location of current heating. Therefore, for stronger radiation heat loss (thinner wires), the absolute value of the phase shift of the 3ω signal becomes smaller.

IV. EXPERIMENTAL DETAILS AND RESULTS

A. Experimental setup

In this work, an experimental setup is established to verify the physical model developed above and to characterize the thermal transport in SWCNT bundles. Since the 3ω voltage ($V_{3\omega}$) signal is small and embedded in the large ω voltage variation over the wire, an experiment using the Wheatstone bridge is designed to distinguish and measure $V_{3\omega}$. The schematic of the experimental setup is presented in Fig. 3. In the diagram, R_s is the sample and R_1 is a rheostat, whereas R_2 and R_3 are large-resistance resistors. Since R_2 and R_3 are large compared to R_s and R_1, most of the current flows through R_s and R_1. In order to avoid heat loss by conduction to the ambient air, the experiment is performed in a vacuum of less than 10^{-3} Torr pressure. At this pressure level, although the density of air is reduced, the mean free path of air molecules is increased to a few centimeters long. Therefore, the thermal conductivity of air of infinite size stays almost the same as that at 1 atm. On the other hand, since the mean free path of air molecules is increased to a few centimeters long, which is three orders larger than the characteristic size (micrometers) of the wire under measurement, the Fourier's law of heat conduction breaks down for the heat transfer from the wire to the ambient air. In fact, a substantial temperature drop will arise at the wire-air interface. This case is similar to that for nanostructures embedded in a medium whose mean free path of energy carriers is much larger than the characteristic size of the nanostructure.[25] The effective thermal conductivity of the air around the wire will be orders of magnitude smaller than that of bulk air. This will make the heat conduction from the wire to air negligible. We have conducted experiments at different vacuum levels and found that the vacuum of 10^{-3} Torr is sufficient to reduce the heat conduction from the wire to air to a negligible level. The cables used are shielded so that external noise may not affect the 3ω amplitude which is at the microvolt level. Before conducting the experiment, R_3 is

tuned to make the ω voltage difference between points A and B minimal. This ensures that the bridge is in balance, and the measured 3ω signal between points A and B has negligible effect from the small 3ω distortion of the heating current. A lock-in amplifier is used to measure the phase shift and amplitude of this 3ω voltage variation. In addition, the sine wave output of the lock-in amplifier is also used as the power source for the experiment.

B. Measurement of microscale Pt wires

Before characterizing the thermophysical properties of SWCNT bundles, the system is calibrated with Pt wires whose properties are known and the size is well defined. In phase shift measurement, the equipment in the experiment will induce some system time delay. In order to rule out the effect of the system time delay, a Pt wire of 25.4 μm diameter and about 5 cm length is taken as the reference for system calibration. This Pt wire is connected between two copper electrodes using silver paste. The electrical resistance of the wire at room temperature is measured to be 11.11 Ω. The phase shift (time delay) induced by the system can be calculated as $\Delta\phi_{\text{sys}}=\phi_{\text{ref}}-\phi_{\text{the}}$, where ϕ_{ref} is the measured phase shift of the reference sample and ϕ_{the} is the theoretical (real) phase shift of the reference sample. After system calibration, the real phase shift of the measured sample is calculated as $\phi_{\text{real}}=\phi_{\text{mea}}-\Delta\phi_{\text{sys}}$.

The length of the reference wire used in our experiment is 4.925 cm. In the experiment, attributed to electrical heating of the wire, its temperature and resistance will be elevated to a higher level T_T and $R_{S,T}$. This *in situ* resistance of the wire is determined as $R_{S,T}=R_1V_{\text{wire}}/V_{R_1}$, with V_{wire} and V_{R_1} being the measured voltage over the wire and rheostat R_1 during the experiment. The increase in temperature over the sample is determined as $T_T=(R_{S,T}-R_0)\pi D^2/4\alpha\rho_0 L$, where R_0 is the resistance over the wire at room temperature, D the diameter of the wire, and α the temperature coefficient of the resistance for Pt.[23] ρ_0 is the resistivity at 0 °C (9.828×10^{-8} Ω m) and L is the length of the wire. The heating power and $V_{3\omega}$ over the wire are determined using the *in situ* resistance of the wire $R_{S,T_T}=4\rho_0L(1+\alpha T_T)/\pi D^2$, which is calculated using the measured wire length to eliminate the effect of electrical contact resistance. After measuring the amplitude of the 3ω signal ($V_{3\omega,\text{meas}}$) between points A and B, as shown in Fig. 3, it is readily found that the real 3ω amplitude ($V_{3\omega}$) over the wire is $V_{3\omega}=[(R_s+R_1)/R_1]V_{3\omega,\text{meas}}$.

Based on the real amplitude $V_{3\omega}$, data fitting is conducted to determine the product of ρc_p for the Pt wire. In this data fitting, since the wire is thick (25.4 μm), the radiation heat loss from the wire surface will have negligible effect on the measured phase shift and amplitude as stated in Sec. III. In this amplitude fitting to determine ρc_p, the thermal conductivity k of the wire is unknown. Different k values are tried to explore how its value affects the fitted ρc_p. Our results prove that ρc_p has a weak dependence on the value of the thermal conductivity. With k changing from 6.6 to 126.6 W/m K, ρc_p changes less than 10%. Figure 4(a) shows the fitting result of $V_{3\omega}$ in comparison with the experimental data. A sound agreement is observed between them.

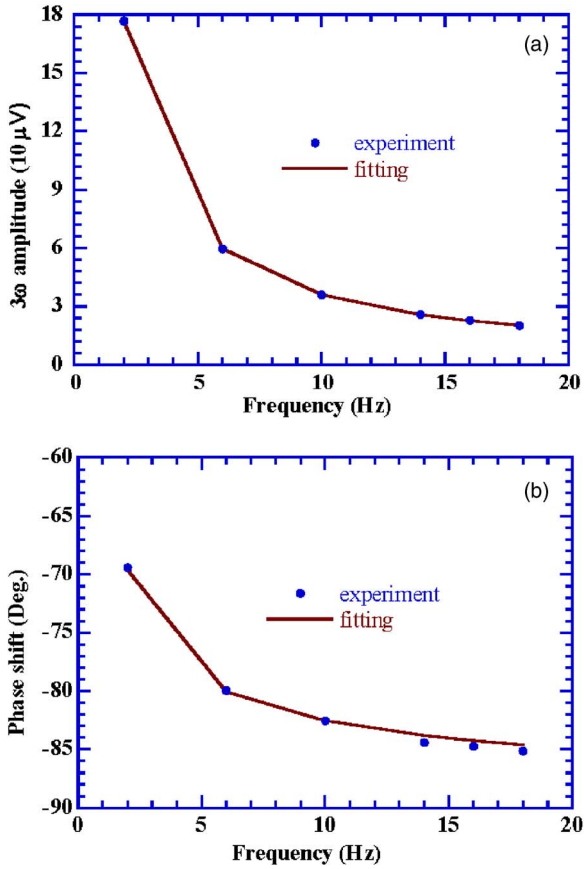

FIG. 4. (Color online) (a) Amplitude fitting for the long (4.925 cm) Pt wire with assumed $k=71.6$ W/m K. The ρc_p value is fitted to be 2.93×10^6 J/m^3 K; (b) phase shift fitting for the short (5.38 mm) Pt wire with $\rho c_p=2.93\times10^6$ J/m^3 K to find the thermal conductivity ($k=71.2$ W/m K).

Based on thermal conductivity $k=71.6$ W/m K value,[24] ρc_p is fitted to be 2.93×10^6 J/m^3 K at an experimental temperature of 60.96 °C. This value is close to the reference value of 2.853×10^6 J/m^3 K[24] with a difference less than 3%.

In our experiment, it is found that ρc_p fitting is sensitive to many parameters, such as the diameter, length, and resistance of the wire. The values of these parameters are either provided by the company or measured in the experiment. The uncertainty in these parameters will propagate to the final fitting result to give rise to uncertainty in the fitted ρc_p. We have conducted extensive experiments for ρc_p fitting and found that longer wires give better result. For longer wires, the connecting region and electrical contact resistance will have relatively smaller effect on the measured length and resistance. Therefore, the final fitted ρc_p is closer to the real value of Pt. In addition, we found that using $V_{3\omega}=[(R_s+R_1)/R_1]V_{3\omega,\text{meas}}$ to calculate $V_{3\omega}$ will induce appreciable uncertainties from the electrical contact resistance when measuring R_s and R_1. This is because when R_s and R_1 are small, such as a few ohms, the electrical contact resistance will become more important. For small R_s and R_1, the following equation is suggested to calculate $V_{3\omega}$: $V_{3\omega}=[(R_2+R_3)/R_2]V_{3\omega,\text{meas}}$. This is because R_2 and R_3 are in the order of megaohms and are much less affected by the electrical contact resistance. Our careful test using $V_{3\omega}=[(R_2+R_3)/R_2]V_{3\omega,\text{meas}}$ confirmed this point.

After the calibration and ρc_p fitting using the long Pt wire, a short Pt wire of 5.38 mm length is measured to determine its thermal conductivity k. Using the fitted value of $\rho c_p = 2.93 \times 10^6$ J/m^3 K the phase shift of the 3ω signal is fitted to determine the thermal conductivity of the Pt wire. Different k values are used to calculate the theoretical phase shift. The k value giving the best fit (least square) of the experimental data is taken as the property of the wire. In this phase shift fitting, the reference sample (long wire) and the short wire sample are measured respectively. Based on the data, the thermal conductivity of the wire is fitted to be 71.2 W/m K at an experimental temperature of 26.48 °C. This value is close to the reference data of 71.6 W/m K (Ref. 24) with a difference less than 1%. Figure 4(b) shows a sound agreement between the fitted phase shift and the experimental data with $k = 71.2$ W/m K.

In the experiment to measure ρc_p for the long Pt wire, the measured amplitude ($V_{3\omega}$) is related to the experimental parameters as $V_{3\omega} \propto I^3 R/(\pi r_0^2 L \rho c_p) dR/dT$. In this work, R and dR/dT are calculated based on the measured length, the temperature increase of the wire, and its electrical resistivity. Considering R, L, and dR/dT, it is readily found that the length of the wire will have first order effect on the measured ρc_p. In the experiment, the length is precisely checked using a caliper. For the 4.925 cm long Pt wire characterized in this work, the length measurement has an uncertainty less than 1%. Therefore, the uncertainty of the measured ρc_p from the length measurement will be below 1%. The diameter of the wire is obtained from the data provided by the industry. Its diameter is also checked under the scanning electron microscopy (SEM). The result shows that for the small section observed under the SEM, the diameter is 25.88 μm, which is only about 1.9% larger than the diameter of 25.4 μm used in data reduction. This will bring about 3.8% uncertainty toward ρc_p. It is expected that the diameter of the Pt wire will have some nonuniformity along its length (some sections a little thicker and some sections a little thinner). Therefore, the overall uncertainty brought into the final result will be less than 3.8%. Since the measured Pt wire is pure Pt, the temperature coefficient of resistance for pure Pt is used. Other possible uncertainty comes from the measurement of the $V_{3\omega}$ signal and temperature increase of the wire. For the $V_{3\omega}$ measurement, the reading for $V_{3\omega,\mathrm{meas}}$ from the lock-in amplifier is very stable and has a small uncertainty (less than 1%) based on our long-time averaging using the computer-controlled data acquisition system. When determining $V_{3\omega}$, as discussed above, the large-resistance R_2 and R_3 are used. Their values are close to 1 MΩ, thereby significantly reducing the effect of electrical contact resistance (approximately in ohms) in the circuit. Therefore, the treatment of $V_{3\omega}$ will bring negligible uncertainty in the final measurement result. When evaluating the temperature increase of the wire during the experiment, the same measurement circuit is applied to both ends of the Pt wire before and during the experiment. The measured resistance before (R_0) and during the experiment (R_s) will consist of the same electrical contact resistance. Their difference ($R_s - R_0$) rules out the contact resistance and is used to determine the temperature increase of the wire. This temperature increase is then used to calculate the real resistance of the wire during the experiment. The uncertainty brought in by this calculation is about 1.3% since the small temperature increase of the wire will have insignificant effect on its total electrical resistance. One major source for the experimental uncertainty is the ambient noise introduced to the system. To check the effect of the noise, different long wires have been measured to determine their ρc_p. It shows that the measured data is always in good agreement with the literature value with a difference less than 10%.

As for the measurement of the thermal conductivity of Pt wires, short wires have to be used in order to enhance the effect of heat transfer on the measured phase shift. Different from the ρc_p measurement, only the length of the wire will have significant effect on the final result. Its diameter will have negligible effect on the measured phase shift and the final data fitting. For the short wire (5.38 mm) used in the measurement, the length measurement will have an uncertainty around 0.1 mm (1.9%), largely induced by the determination of the contact point between the wire and the electrodes. From Eq. (9) it is seen that the length is related to the thermal conductivity in the form of $\sqrt{\rho c_p 2i\omega/k}L$. It is not difficult to find that the 1.9% uncertainty in the length measurement will introduce about 3.8% uncertainty to the measured thermal conductivity. In addition to length measurement, noise from the outside will introduce inevitable uncertainty to the measured phase shift. To address this issue, the experiment has been conducted at different times to evaluate the effect of the noise. It indicates that the measurement repeatability can be well controlled to be better than 10%.

C. Thermal characterization of SWCNT bundles

In this section, bundles consisting of SWCNTs are measured using the established 3ω technique. Centimeter-long ropes of well-aligned SWCNTs were synthesized using a H_2/Ar arc discharge method. The synthesis process is described in detail by Liu *et al.*[26] In brief, Ar and H_2 gases were introduced into a vacuum chamber as buffer gases. The cathode was a graphite rod with the tip sharpened. The anode was a graphite cylinder with holes filled by evenly dispersed graphite powder, Fe–Ni–Co (as catalyst), and a sulfur-containing growth promoter. An angle between the axes of the two electrodes was set at 30°–50°. When an electric arc is initiated, the SWCNT strands can be obtained on the collectors installed in the reaction chamber.

Before characterizing their thermophysical properties, we first study the structure of the to-be-measured SWCNT bundles. Figure 5 shows the SEM pictures of SWCNT bundles with different resolutions. From Fig. 5(a), it is seen that the diameter of the SWCNT bundle is over 40 μm. At this scale, the radiation heat loss from the bundle surface has negligible effect on the measured 3ω signal. Figure 5(b) shows the threads inside the bundle. Various size pores exist in the bundle. The orientation of the SWCNTs does not follow the axial direction of the bundle. It is anticipated that the random orientation of the SWCNTs and the pores inside can significantly reduce the thermal conductivity of the bundle.

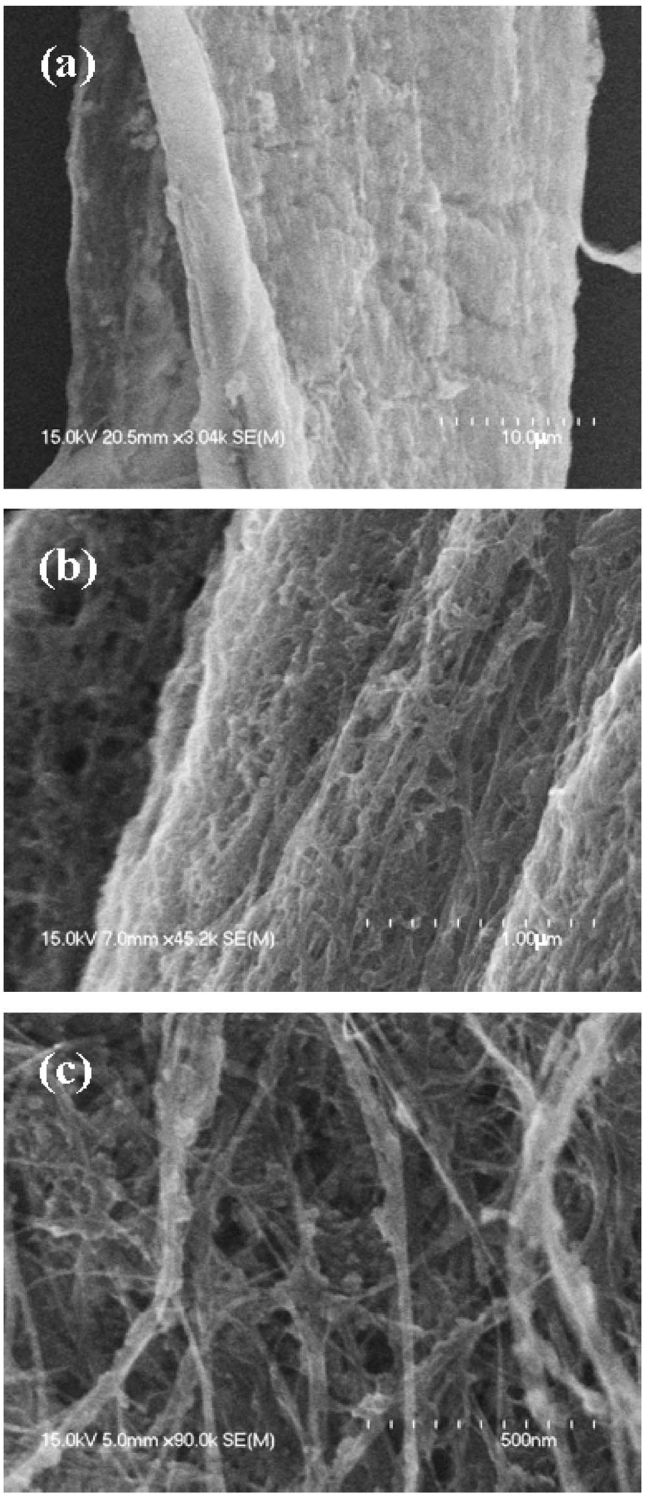

FIG. 5. SEM images of the characterized SWCNTs: (a) a low resolution image showing the overall bundle thickness, (b) high-resolution image showing the threads inside the bundle, and (c) higher-resolution image showing the diameter of individual SWCNT threads.

Figure 5(c) tries to illustrate the diameter of the SWCNT threads. It is observed that the diameter of the visible SWCNT threads varies from less than 10 nm to a few tens of nanometers. To confirm the existence of SWCNTs, Raman scattering is conducted for the sample. The Raman spectrum of the bundle is shown in Fig. 6. The peak at 1341 cm^{-1} indicates that the sample has graphitic networks of finite size

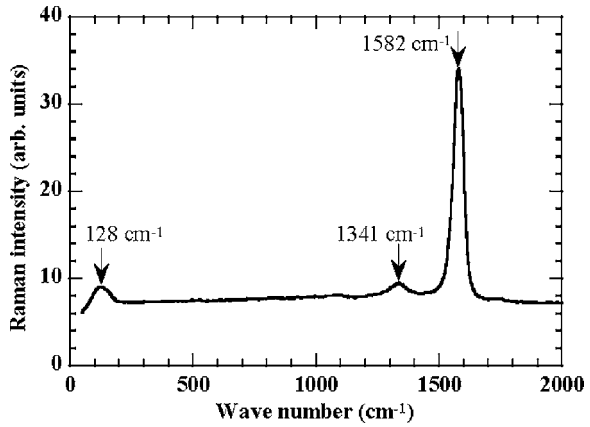

FIG. 6. Raman scattering spectrum for the measured SWCNT bundles.

(<100 nm) or defects. This has been studied and confirmed in the past.[27] In comparison with the Raman peak for the E_{2g} (stretching) mode in graphite (1580 cm^{-1}), the Raman scattering in Fig. 6 shows left shift of this peak (1582 cm^{-1}). This shift is induced by some physical mechanisms inherent to nanotubes of different radii. A high resolution Raman scattering study of SWCNTs has revealed splitting of the E_{2g} mode peak due to the existence of SWCNTs.[26,27] The low-frequency peak at 128 cm^{-1} is associated with the radial breathing mode of SWCNTs and can be used to evaluate the tube diameter.[28,29] Based on the peak location, it is estimated that the primary diameter of SWCNTs in the bundle is $d=223.75(cm^{-1}\ nm)/128\ cm^{-1}=1.75$ nm. Therefore, the threads observed in Fig. 5(c) are comprised of many SWCNTs.

For thermal transport characterization, the to-be-measured SWCNT bundle is connected between two copper electrodes using silver paste. Table II shows the length and resistance of the three SWCNT bundles measured in the experiment. The typical thickness/diameter of the SWCNT bundle is measured to be around 20 μm. Under this condition, radiation heat loss from the bundle surface will have negligible effect on the measured 3ω signal. In the 3ω experiment, in order to make the experimental principles valid, the sample has to be an electrical conductor. For SWCNTs, the diameter and felicity are uniquely characterized by the vector $C_h=n\mathbf{a}_1+m\mathbf{a}_2\equiv(n,m)$ that connects crystallographically equivalent sites on a two-dimensional (2D) graphene sheet, where $\mathbf{a}_1$ and $\mathbf{a}_2$ are the graphene lattice vectors and n and m are integers. The SWCNT will be the conductor when $n-m$ is divisible by 3.[30] Before the experiment, the I-V characteristic of the sample is checked. The results confirm that within the experimental voltage range (−0.3–0.3 V), the

TABLE II. Details of three different SWCNT samples characterized in the experiment.

	Sample 1	Sample 2	Sample 3
Length (mm)	1.828	1.143	1.905
Resistance (Ω)	122.0	223.0	100.0
Measured thermal diffusivity (10^{-6} m^2/s)	12.7	19.8	19.7

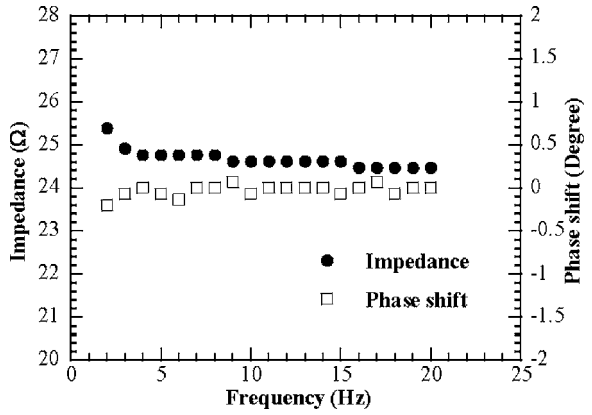

FIG. 7. Impedance spectrum for the SWCNT bundles in the frequency range of 2–20 Hz.

I-V curve for the samples is linear, demonstrating the metallic behavior. In addition to the *I-V* characteristic, the SWCNT bundle is modeled as resistance, capacitor, and inductor connected in parallel to check its capacitance and inductance. Similar to the work by Choi *et al.*[31] for multiwall CNTs, experiments are conducted at different frequencies to measure the impedance of the SWCNT bundle and the phase lag between the current and voltage over it. The measurement results are shown in Fig. 7. In the frequency range of 2–20 Hz, the impedance stays nearly the same as the dc resistance of 24.4 Ω. The phase shift between the current and voltage is close to 0. The largest phase shift is less than 0.3°. It demonstrates that in the frequency range of 2–20 Hz, the capacitance and inductance of the SWCNT bundle have negligible effect on the 3ω experiment.

Since we do not have the exact diameter of the SWCNT bundle and the dependence of its resistance over the temperature, ρc_p of the SWCNT bundle becomes difficult to determine based on the experimental data. Instead, the thermal diffusivity of the sample is characterized based on the phase shift of the 3ω signal. Figure 8 shows the fitted phase shift versus the experimental data for sample 3. In this fitting, ρc_p takes 0.184×10^6 J/m^3 K and the thermal conductivity k is fitted to be 3.58 W/m K. It needs to be pointed out that for each assumed ρc_p, one k can be found to fit the experimental data. For the three samples measured in the experiment, different values of ρc_p are used to fit the thermal conductivity. From the plot of the $k \sim \rho c_p$ curve for the three samples, the slope of each curve is utilized to obtain the thermal diffusivity, as stated in Table II. Their values are 12.7, 19.8, and 19.7×10^{-6} m^2/s, respectively. It is clear that the thermal diffusivity of the three samples is in the same order. The difference among them is probably attributed to different alignments of the tube bundles and tube structural characteristics. The average thermal diffusivity of the above three different SWCNT samples is around 17.4×10^{-6} m^2/s. This value is much smaller than the thermal diffusivity of graphite 1.24×10^{-3} m^2/s in the layer direction.[24] This measured small thermal diffusivity of SWCNT bundles is attributed to several characteristics of the bundle structure. First, as we discussed above (shown in Fig. 5), the SWCNT threads in the bundle do not follow its axial direction. This random orientation can substantially reduce the thermal conductivity of the material. Second, the contact between the threads (shown in Fig. 5) will give rise to an appreciable thermal contact resistance, which can significantly reduce the thermal transport in the bundle. Finally, possible defects in the SWCNTs themselves can reduce their thermal conductivity and give contribution to the measured low thermal diffusivity.

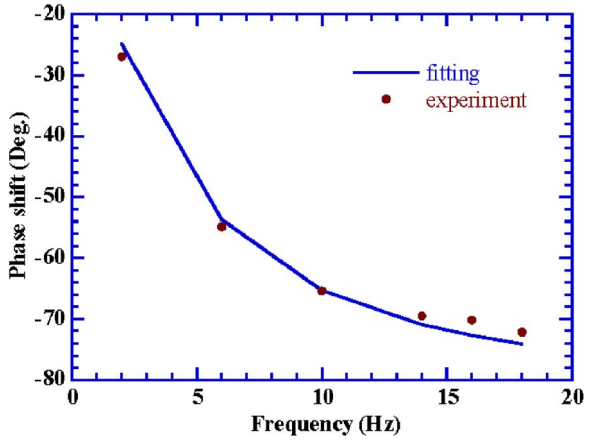

FIG. 8. (Color online) Phase shift of sample 3 vs the fitting result.

V. CONCLUSION

In this work, the thermal transport in the 3ω experiment for thermal characterization of individual wires was studied by developing a comprehensive analytical solution that took into account the thermal contact resistance, heat transfer in the electrode base, and radiation heat loss from the wire surface. Our study showed that for wires with a diameter around 100 nm or thinner, the radiation heat loss from the wire surface will have a strong effect on the amplitude and phase shift of the 3ω signal. This influence became stronger for thinner wires. Experiments were conducted to verify the physical model by measuring the ρc_p and k of Pt microwires. The fitted ρc_p and thermal conductivity of the Pt wire agreed well with reference values. The thermal diffusivity of SWCNT bundles of different lengths was measured using the established experiment. Their average value is 1.74×10^{-5} m^2/s, much smaller than the thermal diffusivity of graphite in the layer direction. This is probably due to the random orientation of SWCNTs in the bundle, the thermal contact resistance between SWCNT threads, as well as some possible structural defects of SWCNTs.

ACKNOWLEDGMENTS

Support for this work from NSF (CTS: 0400458), the Nebraska Research Initiative, the MURI Grant from ONR, and the Layman Award of the University of Nebraska-Lincoln (UNL) is gratefully acknowledged. Support from Dr. Yongfeng Lu and Kaijun Yi of the Department of Electrical Engineering at UNL for measuring the Raman spectrum of the SWCNT bundles is very much appreciated.

[1] L. Chico, V. H. Crespi, L. X. Benedict, S. G. Louie, and M. L. Cohen, Phys. Rev. Lett. **76**, 971 (1996).
[2] L. Langer *et al.*, Phys. Rev. Lett. **76**, 479 (1996).

[3]T. W. Ebbesen, H. J. Lezec, H. Hiura, J. W. Bennett, H. F. Ghaemi, and T. Thio, Nature (London) **382**, 54 (1996).
[4]T. Pichler, M. Knupfer, M. S. Golden, J. Fink, A. Rinzler, and R. E. Smalley, Phys. Rev. Lett. **80**, 4729 (1998).
[5]E. W. Wong, P. E. Sheehan, and C. M. Lieber, Science **277**, 1971 (1997).
[6]S. G. Volz and G. Chen, Appl. Phys. Lett. **75**, 2056 (1999).
[7]A. Khitun, A. Balandin, and K. L. Wang, Superlattices Microstruct. **26**, 181 (1999).
[8]S. Berber, Y. K. Kwon, and D. Tomanek, Phys. Rev. Lett. **84**, 4613 (2000).
[9]L. Shi, D. Li, C. Yu, W. Jang, D. Kim, Z. Yao, P. Kim, and A. Majumdar, J. Heat Transfer **125**, 881 (2003).
[10]J. Hone, M. Whitney, C. Piskoti, and A. Zettl, Phys. Rev. B **59**, R2514 (1999).
[11]J. Hone *et al.*, Appl. Phys. Lett. **77**, 666 (2000).
[12]W. Yi, L. Lu, D. Zhang, Z. W. Pan, and S. S. Xie, Phys. Rev. B **59**, R9015 (1999).
[13]X. Wang, Z. Zhong, and J. Xu, J. Appl. Phys. **97**, 064302 (2005).
[14]A. Mizel, L. X. Benedict, M. L. Cohen, S. G. Louie, A. Zettl, N. K. Budraa, and W. P. Beyermann, Phys. Rev. B **60**, 3264 (1999).
[15]D. G. Cahill, Rev. Sci. Instrum. **61**, 802 (1990).
[16]S. M. Lee and D. G. Cahill, J. Appl. Phys. **81**, 2590 (1997).
[17]S. M. Lee, D. G. Cahill, and R. Venkatasubramanian, Appl. Phys. Lett. **70**, 2957 (1997).
[18]J. H. Blackwell, J. Appl. Phys. **25**, 137 (1954).
[19]P. Andersson and G. Backstrom, Rev. Sci. Instrum. **47**, 205 (1976).
[20]S. E. Gustafsson and E. Karawacki, Rev. Sci. Instrum. **54**, 744 (1983).
[21]L. Lu, W. Yi, and D. L. Zhang, Rev. Sci. Instrum. **72**, 2996 (2001).
[22]T. Y. Choi, D. Poulikakos, J. Tharian, and U. Sennhauser, Appl. Phys. Lett. **87**, 013108 (2005).
[23]*Handbook of Chemistry and Physics*, 64th ed. (CRC, Boca Raton, FL, 1983), p. F-125.
[24]F. P. Incropera and D. Dewitt, *Fundamentals of Heat and Mass Transfer*, 5th ed., (Wiley, New York, 2002).
[25]G. Chen, J. Heat Transfer **118**, 539 (1996).
[26]C. Liu, H. M. Cheng, H. T. Cong, F. Li, G. Su, B. L. Zhou, and M. S. Dresselhaus, Adv. Mater. (Weinheim, Ger.) **12**, 1190 (2000).
[27]A. Kasuya, Y. Sasaki, Y. Saito, K. Tohji, and Y. Nishina, Phys. Rev. Lett. **78**, 4434 (1997).
[28]E. Richter and K. R. Subbaswamy, Phys. Rev. Lett. **79**, 2738 (1997).
[29]S. Bandow, S. Asaka, Y. Satio, A. M. Rao, L. Grigorian, E. Richter, and P. C. Eklund, Phys. Rev. Lett. **80**, 3779 (1998).
[30]W. Zhang, Z. Zhu, F. Wang, T. Wang, L. Sun, and Z. Wang, Nanotechnology **15**, 936 (2004).
[31]T. Y. Choi, D. Poulikakos, J. Tharian, and U. Sennhauser, Nano Lett. **6**, 1589 (2006).